Use of Parsons-Lee and Onsager theories to predict nematic and demixing behavior in binary mixtures of hard rods and hard spheres

Alejandro Cuetos
Soft Condensed Matter, Utrecht University, Princetonplein 5, 3584 CC Utrecht, The Netherlands

Bruno Martínez-Haya* and Santiago Lago
Departamento de Sistemas Físicos, Químicos y Naturales, Universidad Pablo de Olavide, 41013 Seville, Spain

Luis F. Rull
Departamento de Física Atómica, Molecular y Nuclear, Area de Física Teórica, Universidad de Sevilla, Apdo. 1065, 41080 Seville, Spain

(Received 21 September 2006; revised manuscript received 26 March 2007; published 4 June 2007)

Parsons-Lee and Onsager theories are formulated for the isotropic-nematic transition in a binary mixture of hard rods and hard spheres. Results for the phase coexistence and for the equation of state in both phases for mixtures with different relative sizes and composition are presented. The two theories explain correctly the general behavior observed in experiments and computer simulations for these fluids. In particular, the theory accounts for the destabilization of the nematic phase when spherical or globular macromolecules are added to a system of rodlike colloids, and the entrance of the system into a demixed regime at high volume fractions of the spherical particles. Upon demixing a nematic state rich in rods coexists in equilibrium with an isotropic state much more diluted in the rodlike component. Onsager theory fails on quantitative grounds for aspect ratios of the rodlike molecules smaller than 100, and in the cases where the molar fractions of spheres becomes close to unity. On the contrary, the Parsons-Lee approximation remains accurate down to aspect ratios as small as 5. The spinodal analysis indicates that the isotropic-isotropic and nematic-nematic coexistences become feasible for sufficiently large spheres and long rods, respectively. The latter type of coexistence interferes partially with the isotropic-nematic coexistence regime of interest to the present work. Overall, the study serves to rationalize and control key aspects of the behavior of these binary nematogenic colloidal systems, which can be tuned with an appropriate choice of the relative size and molar fractions of the particles.

DOI: 10.1103/PhysRevE.75.061701 PACS number(s): 64.70.Md, 61.30.Cz, 83.80.Xz, 87.15.Aa

I. INTRODUCTION

One of the aims of statistical mechanics is to establish a link between molecular interactions and phase behavior. This is a particularly difficult task in the field of liquid crystals, due the anisotropy of the molecular shapes and interactions, which are the essential features retained even in the most simple models. The major importance of molecular shape has nowadays become a consolidated aspect with interdisciplinary recognition. Properties such as the stability of colloidal suspensions or the conformational behavior of polymeric systems can be controlled with the addition of particles with the appropriate shape and molar fraction. In biological sciences, it has been established that excluded volume effects play an essential role in the equilibrium and dynamical properties of macromolecules in physiological environments [1,2].

Historically, Onsager [3] and Maier and Saupe [4] pioneered the study of liquid crystals since the early 1940's. The original works of Onsager have been revised by several authors [5–10] and have been applied to the study of fluid mixtures involving rodlike and platelike particles [11–16]. Onsager theory, despite its inherent limitations, presents one fundamental advantage with respect to its more accurate counterparts. The simple second virial approximation on which the theory relies, provides an intuitive framework for the understanding of the physical problem in terms of the steric effects associated to the particular molecular geometries considered. For finite size molecules, Onsager theory tends to become inaccurate at the high densities typical of liquid crystal transitions, and numerous more refined approaches have been developed [17–19]. Among these, Parsons-Lee [20,21] and scaled particle [22] theories have been of historical importance. One of the most extensive theoretical studies to date of the global phase diagram of polydispersed rodlike particles has been reported by Velasco, Mederos, and co-workers from Parsons-Lee and density functional theories [23–25]. These authors characterized in detail the phase diagram of mixtures of hard rods of different sizes but devoted, however, limited attention to the specific case of the rod/sphere mixture object of the present work.

In the present article, we outline an application of Onsager and Parsons-Lee theories to the particular case of the binary mixture of spherical and rodlike colloids, modeled by hard spheres (HS) and hard spherocylinders (HSC), respectively. This kind of mixtures have received considerable attention in recent years, mainly within the context of the stability of colloidal suspensions [27–31]. Although the liquid crystal properties of these binary mixtures have been more scarcely investigated, significant contributions have been made to this respect from the experimental and theoretical points of view. The wealth of the phase behavior of these systems has been extensively demonstrated experimentally

*Email address: bmarhay@upo.es

by Fraden and co-workers [19,32–36], as well as by other groups [37–39]. Experiments typically employ mixtures of spherical colloids or globular polymers with rodlike particles, such as the Tobacco Mosaic virus [19,33], the bacteriophage *fd* virus [32], nanorods of cellulose [37], and boehmite [38] or organic liquid crystals [39–42]. The *fd* virus, in particular, depending on environmental parameters such as pH or ionic strength, can have effective length-to-breadth ratios ranging from a few tens to up to around 100. This latter value has been established as a rough limit for the accurate applicability of Onsager theory for pure fluids of prolate molecules [19].

Interestingly, much of the rich phenomenology observed experimentally remains to a large extent unexplained, although some relevant effects have been reproduced in theoretical and computer simulation studies [23–26,30,43–46]. The main motivation of the current contribution is the elucidation of the capability of Onsager and Parsons-Lee theories (presented in Sec. II) for predicting, on qualitative and quantitative grounds, nematic ordering and demixing transitions in rod-sphere binary mixtures. Perhaps surprisingly, a systematic study of this nature has not been performed up to date for rod-sphere mixtures.

II. THEORY

The Onsager theory for the HSC-HS binary mixture here outlined represents an extension of the original approach to the free energy for the pure rod system [3]. It complements similar approaches applied previously to mixtures of rodlike molecules without specific attention to rod-sphere mixtures [5,13].

Onsager treated the pure rod system formally as a polydispersed mixture by considering particles with different orientations in space as belonging to different molecular species [3]. It was assumed that the probability distribution for the orientation of the rodlike particles with respect to a fixed frame is determined by a single-particle distribution function $f(\Omega)$. In the isotropic phase all orientations are equally probable so that $f(\Omega)=(4\pi)^{-1}$, whereas in the nematic phase, due the axial symmetry of the particles, $f(\Omega)=(2\pi)^{-1}h(\theta)$, θ being the angle between the molecule and the nematic director vector.

Onsager's approach provides a natural means of introducing the spherical particles in the theory, namely, as one additional species of the formal multicomponent mixture constituted by the HSC particles with different orientations. With these premises, a mimic of the procedure followed by Onsager leads to the following expression for the free energy of the binary mixture of N_c freely rotating hard spherocylinders and N_s spheres:

$$\frac{\beta F}{N} = f_{\text{iso}}^{\text{id}} + f_1 + f_2, \tag{1}$$

$$f_1 = -1 + \ln \rho + x_c \sigma[f] + x_c \ln x_c + x_s \ln x_s, \tag{2}$$

$$f_2 = \sum_{ij} x_i x_j \frac{\rho}{2} \int \int d\Omega_i d\Omega_j f(\Omega_i) f(\Omega_j) v_{\text{exc};ij}(\Omega_i, \Omega_j) \tag{3}$$

with

$$\sigma[f] \equiv \int f(\Omega) \ln[4\pi f(\Omega)] d\Omega. \tag{4}$$

In the above equation, N is the total number of particles, ρ the particle density, x_c and x_s denote the molar fractions of HSC and HS particles, and $f_{\text{iso}}^{\text{id}}$ is the concentration-independent part of the free energy per particle in units of thermal energy $\kappa T=\beta^{-1}$. The subscripts i,j run on the types of particles in the mixture, i.e., spherocylinders and spheres. The functions $v_{\text{exc};ij}(\Omega_i,\Omega_j)$ denote the physical volume of space mutually excluded between pairs of HSC-HSC, HSC-HS, and HS-HS particles, which will be henceforth denoted by v_{cc}, v_{cs}, and v_{ss}, respectively:

$$v_{cc}(\gamma) = 2L^2\sigma|\sin\gamma| + 2\pi\sigma^2 L + (4/3)\pi\sigma^3 \equiv \frac{8}{\pi} a|\sin\gamma| + v_{ca}, \tag{5}$$

$$v_{cs} = \pi\left[\frac{(D+\sigma)^3}{6} + \frac{(D+\sigma)^2}{4} L\right], \tag{6}$$

$$v_{ss} = \frac{4}{3}\pi D^3. \tag{7}$$

Here, L and σ stand for the length and diameter of the HSC particles, respectively, D is the diameter of the HS particles, and $\gamma(\Omega_i,\Omega_j)$ is the angle between the axes of the HSC particles.

We introduce at this point the Parsons-Lee formulation for the rod-sphere mixture, in which a scaling approximation is considered that takes effectively into account higher virial coefficients than Onsager theory [20,21,47]. Within the Parsons-Lee approximation, the integration of the virial equation for the pressure leads to an expression for the free energy of the HSC-HS binary mixture similar to Eq. (1) with

$$f_2 = -\frac{1}{6}\sum_{ij} x_i x_j \int d\rho \int d\mathbf{r} \int \int d\Omega_i d\Omega_j f(\Omega_i) f(\Omega_f) g_{ij}(\mathbf{r},\Omega_i,\Omega_j)[\beta\nabla_r V_{ij}(\mathbf{r},\Omega_i,\Omega_j)\cdot\mathbf{r}] \tag{8}$$

$$\approx -\frac{1}{2}\int d\rho g_{\text{HS};vm} \sum_{ij} x_i x_j \int \int d\Omega_i d\Omega_j f(\Omega_i) f(\Omega_j) v_{\text{exc};ij}(\Omega_i,\Omega_j), \tag{9}$$

where V_{ij} is the intermolecular potential between a pair of particles i and j. For hard core interactions, such as the ones presently considered, an additional approximation must be assumed in order to obtain an expression for the radial distribution functions at contact between the different molecular components $g_{ij}(\sigma_{ij})$ (with σ_{ij} being the pair contact distance). Such contact values arise from the integration of the $\delta(r-\sigma_{ij})$ functions given by the gradient of the discontinuous V_{ij} potential. One of the simplest choices consists of assuming $g_{ij}(\sigma_{ij})=g_{\mathrm{HS};vm}$ for all relative pair orientations. Here, $g_{\mathrm{HS};vm}$ stands for the contact value of a pair of hard spheres with effective diameters corresponding to the same average molecular volume v_m as the mixture under study. For the present case, $v_m=x_s v_s+x_c v_c$, where v_c and v_s denote the molecular volumes of the HSC and HS particles, respectively. The introduction of this approximation into Eq. (8) leads to the above Eq. (9). Even though several more complex functionalities for $g_{ij}(\sigma_{ij})$ were tested within the present work, none of them yielded a better agreement between theory and simulation.

The integral on the density in Eq. (9) is solved by means of the Carnahan-Starling equation for the compressibility of the HS fluid Z_{HS} [48]:

$$\hat{f}(\eta;v_m) \equiv \int d\rho g_{\mathrm{HS};vm} = \int d\rho \frac{Z_{\mathrm{HS}}-1}{4\eta} = \frac{1}{v_m}\frac{4\eta-3\eta^2}{(1-\eta)^2}, \tag{10}$$

where $\eta=\rho v_m$ denotes the packing fraction of the system.

The combination of the different expressions outlined above leads to the following compact formulation for the free energy of the HSC-HS mixture within the Onsager and Parsons-Lee approximations

$$\frac{\beta F}{N} = f_{\mathrm{iso}}^{\mathrm{id}} - \{1-\ln\rho-(x_c\ln x_c + x_c\sigma[f]) - x_s\ln x_s - \Lambda(x_c^2(2ag[f]+v_{ca})+2x_c x_s v_{cs}+x_s^2 v_{ss})\} \tag{11}$$

with

$$g[f] \equiv \frac{4}{\pi}\int |\sin\gamma| f(\Omega) f(\Omega') d\Omega'$$

and

$$\Lambda = \frac{\rho}{2}\ \text{(Onsager) or}\ \Lambda = \frac{\hat{f}(\eta;v_m)}{8}\text{(Parsons-Lee)}. \tag{12}$$

In the limit $L^*\gg 1$, $L^*\gg D^*$ (where $L^*=L/\sigma$ and $D^*=D/\sigma$), the Parsons-Lee expression for Λ converges to the Onsager form and, hence, becomes exact.

One of the most crucial aspect in both Onsager and Parsons-Lee theories is the determination of the orientation distribution function $f(\Omega)$ [or $h(\theta)$ for axial-symmetric systems], which minimizes the free energy of the system. Several functional forms and variational parameters have been proposed for this purpose [3,8,49,50]. In this work, we have followed the alternative approach of minimizing the free energy with respect to variations in $f(\Omega)$ [10], which leads to the integral equation

$$\ln[4\pi f(\Omega)] = \lambda - \Lambda\frac{16ax_c}{\pi}\int |\sin\gamma(\Omega,\Omega')| f(\Omega) d\Omega. \tag{13}$$

Here, λ is the Lagrange multiplier, which is determined by the normalization condition. Equation (13) has always the isotropic phase solution $f(\Omega)=(4\pi)^{-1}$. For the calculation of the nematic phase solution, we have applied a well-known self-consistent methodology [5,51]. The method is based on the even Legendre expansions of $h(\theta)$ and of $|\sin\gamma|$, which by making use of the addition theorem of the Legendre polynomials, and integrating Eq. (13) on the azimuthal angle, leads to the following expression for the distribution function:

$$h(\theta) = \sum_{n=0}^{\infty} a_{2n}P_{2n}(\cos\theta) = K\exp\left[-32ax_c\Lambda\sum_{n=0}^{\infty}\frac{2}{2(2n)+1}a_{2n}d_{2n}P_{2n}(\cos\theta)\right], \tag{14}$$

where K is a normalization constant, a_{2n} are the Legendre expansion coefficients for $h(\theta)$, and d_{2n} are the (analytical) Legendre coefficients for $|\sin\gamma|$ [52].

In order to determine the function $h(\theta)$ of minimum free energy for a given density and molar fraction, Eq. (14) is solved iteratively until self-consistent convergence is obtained in the a_n expansion coefficients. A convergence test revealed that terms up to $2n=20$ had to be included.

Once a converged solution for $h(\theta)$ has been obtained, the different thermodynamic quantities for the HSC-HS fluid can be calculated from the corresponding partial derivatives of the free energy. In particular, it is worthwhile to notice that the equation of state is given by the following expression:

$$\beta p = \rho + \rho^2\frac{d\Lambda}{d\rho}\{x_c^2(2ag[f]+v_{ca})+2x_c x_s v_{cs}+x_s^2 v_{ss}\} \tag{15}$$

which becomes fully analytical in the isotropic phase, where $g[f]=1$.

The coexistence between the isotropic and nematic phases can be characterized by solving the system of equations $p^I=p^N$, $\mu_c^I=\mu_c^N$, and $\mu_s^I=\mu_s^N$, where the superscripts I and N indicate the isotropic and nematic phases, respectively. In this system of equations, the unknown quantities are the packing fractions of the two phases and the molar fraction of spherocylinders in the nematic phase x_c^N. The choice of x_c^I instead of x_c^N led to equivalent results but with a slower convergence of the iterative method. The numerical solution to the coexistence equations was carried out following the procedure outlined in Ref. [51]. Only for the fluids of shorter particles ($L^*\leqslant 20$) the present work employs the more efficient genetic algorithm described in the appendix below.

We finally describe an extension of the methodology outlined above in order to incorporate an evaluation of the range of stability of the *I-I* and *N-N* phase coexistences in the

HSC-HS fluid. In a pioneering study based on scaled particle theory, Lekkerkerker and Stroobants characterized these types of coexistence for binary mixtures of hard rods and polymers [54]. It will be shown that within the HSC-HS geometries scoped in the present work, the *I-I* coexistence is not relevant and the *N-N* coexistence becomes stable for a well delimited range of particle geometries. Otherwise, the phase diagram will be dominated by *I-N* coexistence, which will therefore constitute the main concern of the investigation.

Spinodal curves delimiting the region of possible occurrence of *I-I* and *N-N* coexistence were calculated extending, to the frame of Parsons-Lee theory, the formalism proposed by van Roij and Mulder within Onsager approximation [12,55], which relies on the stability conditions of a mixture in a thermodynamic phase expressed as

$$\left(\frac{\delta^2 \beta F/N}{\delta v^2}\right)_x > 0,$$

$$\left(\frac{\delta^2 \beta F/N}{\delta x^2}\right)_v > 0,$$

$$\left(\frac{\delta^2 \beta F/N}{\delta v^2}\right)_x \left(\frac{\delta^2 \beta F/N}{\delta x^2}\right)_v - \left(\frac{\delta^2 \beta F/N}{\delta x \delta v}\right)^2 > 0, \qquad (16)$$

where x is the molar fraction of one of the components and $v=1/\rho$. The application of the above inequalities to the Parsons-Lee expression for the free energy given by Eq. (11), with $\Lambda=\hat{f}(\eta;v_m)/8$, leads to lengthy expressions which are, however, straightforward to obtain. The explicit dependence of Λ on the composition of the mixture through v_m must be taken into account. This is in contrast to Onsager theory where Λ is only dependent on ρ.

If any one of the three inequalities of Eq. (16) becomes negative the homogeneous mixing of the binary system becomes unstable and, consequently, a demixing transition is produced. Hence, the spinodal curve in a given binary mixture separates the region of the phase diagram where the inequalities of Eq. (16) are fulfilled from the region where any of the three inequalities is not satisfied. For the present study, the spinodal was determined in an overwhelming majority of cases by the last inequality, which combines the mixing and mechanical stabilities of the system. Only occasionally the second inequality (mixing equilibrium) was found to be limiting. No evidence for breaking of the mechanical stability condition expressed by the first inequality was detected.

III. RESULTS AND DISCUSSION

Figure 1 illustrates typical isotropic-nematic coexistence diagrams predicted by Parsons-Lee theory for the HSC-HS mixture. The graphs depict the packing fractions, $\eta=\rho v_m$, of the coexisting isotropic and nematic states plotted as a function of the volumetric fraction of spheres $x_v \equiv x_s v_s/v_m$ in each of the phases. The particular cases of HSC with $L^*=300$, 20, and 5 and HS with $D^*=10$, 2, and 1, respectively, are chosen to illustrate the behavior of different molecular geometries. In each of the η-x_v diagrams tie lines joining some of the coexisting states are drawn for reference.

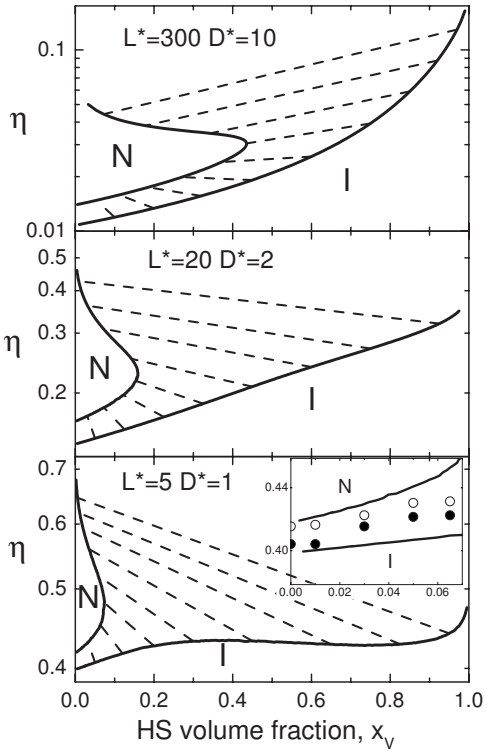

FIG. 1. Typical isotropic-nematic coexistence diagrams predicted by Parsons-Lee theory for the HSC-HS fluid. The packing fractions are represented versus the volumetric fraction of spheres $x_v=(x_s v_s)/v_m$ in the coexisting isotropic and nematic states. Tie lines joining some of the coexisting states are included for illustration. The results shown correspond to binary mixtures with the values for $L^*=L/\sigma$ and $D^*=D/\sigma$ indicated in each panel. The inset in the bottom panel compares the Parsons-Lee coexistence curves with the isotropic (solid symbols) and nematic (open symbols) boundary states reported in Ref. [43] from Monte Carlo (*NPT*-MC) simulations at constant composition.

A first inspection of Fig. 1 already reveals the occurrence of two different coexistence regimes for any given molecular geometry. In the low x_v region, the isotropic and nematic branches evolve close to each other and present only a slight composition asymmetry. On the other hand, as the concentration of spheres is sufficiently increased, a turning point is observed, where the nematic branch attains a maximum x_v value. Beyond the turning point, the binary fluid enters a demixed coexistence regime with a very asymmetric molar fraction of the two components in the isotropic and nematic states. This leads to a phase diagram with a reentrant nature; at (fixed) low volume fraction of spheres, upon increasing η the system evolves from the isotropic phase to a *I-N* coexistence region, then to a nematic region and again to a *I-N* coexistence region. For the HSC-HS systems of Fig. 1 with $L^*=300$, 20, and 5, the nematic coexistence branch reaches maximum values of $x_v \approx 0.43$, 0.16, and 0.074, respectively. In fact, as the isotropic branch evolves to the limit $x_v \to 1$, the volumetric fraction of spheres in the corresponding nematic

state of coexistence becomes progressively smaller and tends to vanish.

In the demixed regime, the relative magnitude of the packing fractions of the coexisting states depends on the relative sizes of the HSC and HS particles. This is noteworthy since in the mixed regime the *I-N* coexistence implies systematically a greater packing fraction in the nematic phase. Figure 1 shows that for $L^*=300$, $D^*=10$ the sphere-rich isotropic branch eventually becomes more compact than its nematic counterpart. For the other two cases $L^*=20$, $D^*=2$ and $L^*=5$, $D^*=1$, the demixed nematic states are always denser than the isotropic ones. Furthermore, the coexistence diagram for $L^*=5$, $D^*=1$ displays a nonmonotonous behavior of the packing fraction in the isotropic branch. It will be shown below that this feature is associated to the demixing regime mixtures with small D/L ratios, where the isotropic branch becomes less dense as it expels HSC particles.

The appearance of highly partitioned isotropic and nematic phases in rod-sphere mixtures was originally predicted theoretically by Flory [53]. In fact, coexistence diagrams in qualitative agreement with the ones shown in Fig. 1 have been observed experimentally for different systems [19,32,33,35–41]. Lekkerkerker and Stroobants [54] described in detail this qualitative behavior for mixtures of colloidal rods and flexible polymers, guided by scaled particle theory. It is therefore gratifying to confirm that Parsons-Lee theory (and also Onsager theory as shown below) captures, at least on qualitative grounds, the behavior observed in real systems on the basis of depletion interaction effects.

Figure 1 also shows that at low values of x_v within the mixed regime, the nematic phase is perturbed by the introduction of spherical particles on the dominant bulk of rodlike particles. Any increment in the fraction of spheres results in a systematic displacement of the *I-N* transition toward higher packing fractions of both coexisting states. This type of retardation of the nematic phase has been found in a recent simulation study of the HSC-HS mixture with $L^*=5$ and $D^*=1$ [43], and appears to be a general effect for small and moderate values of x_v. Figure 1 (bottom panel) illustrates the fair agreement existing between the Parsons-Lee coexistence diagram and the *NPT*-MC simulation data of Ref. [43] in the small x_v regime ($x_v<0.07$) for the particular case of the $L^*=5$, $D^*=1$ mixture. A similar level of quantitative agreement is found for the coexistence pressures (not shown). Figure 2 shows snapshots corresponding to *NPT*-MC simulations of nematic states for the $L^*=5$, $D^*=1$ HSC-HS fluid with x_v values in the mixed and demixed regimes. The simulations corroborate the theoretical predictions by showing that the mixed case maintains the bulk structure of the nematic phase of the pure HSC fluid, whereas a clear segregation of the rodlike and spherical molecules takes place at high x_v.

A question that emerges at this point is whether the demixing transitions predicted in the present theoretical treatment are stable with respect to liquid crystalline transitions other than the nematic one. The most plausible situation to this respect would be the entrance of the fluid into a lamellar phase in which the HSC and HS particles arrange in alternate layers. Phases of this kind have been investigated previously [23–25,43,44]. For the $L^*=5$, $D^*=1$ HSC-HS fluid it has been shown that the lamellar phase becomes stable at packing fractions in the range $\eta=0.45-0.50$, which overlaps with the demixing regime found in the present study for the *I-N* coexistence of that particular mixture. In fact, in the snapshot for the demixed state shown in Fig. 2 it can be appreciated that the segregated HSC particles are more tightly packed than a typical nematic phase and display an arrangement more related to a smectic or solidlike phase. Hence, the application of the present theory, in which the demixing transitions are treated within the context of nematic ordering is limited to HSC elongations greater than $L^*=5$. Fortunately, as L^* is increased the transition to the lamellar phase is also delayed to greater packing fractions and, in addition, the demixed nematic regime takes place at smaller packing fractions (see Fig. 1). In this way, for the particular case of $L^*=20$, the smectic A phase becomes stable at $\eta\approx 0.5$ [58], a value well above the range where the *I-N* demixing occurs (see Fig. 1). It follows that the conclusions related to the demixing behavior of the HSC-HS fluid drawn from the present theoretical treatment are expected to be robust, within the framework of the Parsons-Lee and Onsager approximations, for mixtures of HSC particles with elongations of $L^*\approx 10-20$ or greater.

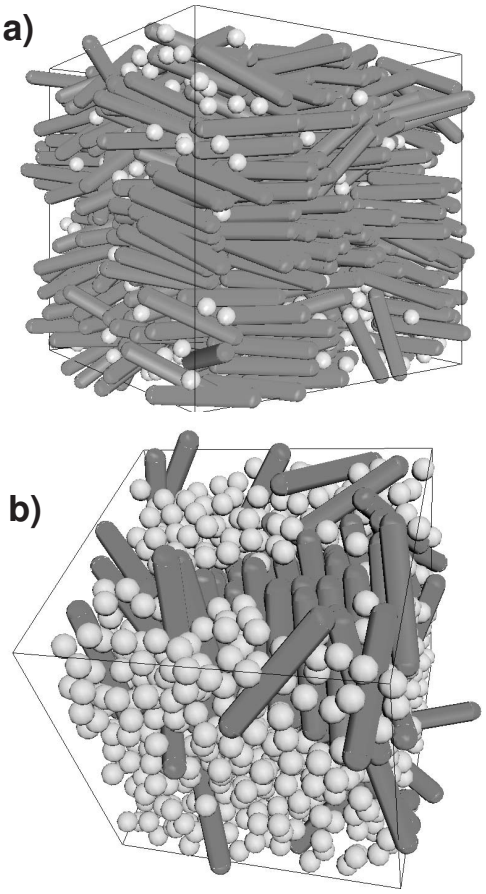

FIG. 2. Snapshots from Monte Carlo simulations of the HSC-HS fluid with $L^*=5$, $D^*=1$ in (a) a mixed nematic state with $x_v=0.065$ and $\eta=0.442$ and (b) a demixed nematic state with $x_v=0.536$ and $\eta=0.412$. The computations were performed as described in Ref. [43].

We will now focus the discussion in more detail on the theoretical predictions for the dependence of the *I-N* coexist-

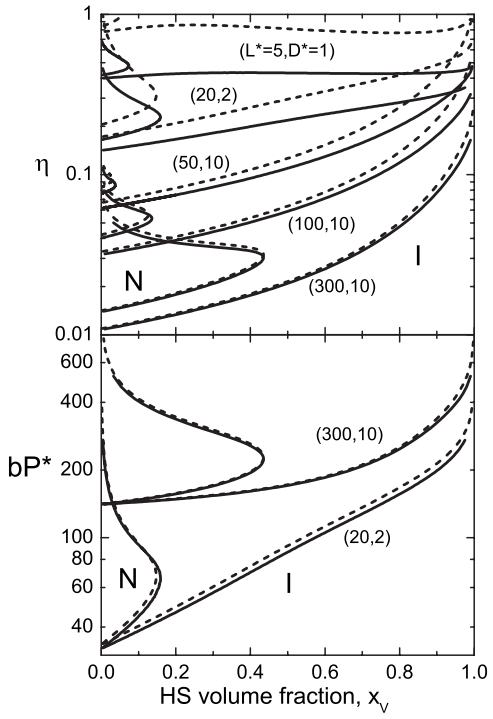

FIG. 3. Isotropic-nematic coexistence diagram predicted by Parsons-Lee (solid curves) and Onsager (dashed curves) theories for HSC-HS fluids with different elongations of the HSC particles L^* and diameters of the HS particles D^* as indicated. The dimensionless pressure of the mixture is defined as $bP^*=b\beta P\sigma^3$, with $b=(\pi/4)L^{*2}D^*$.

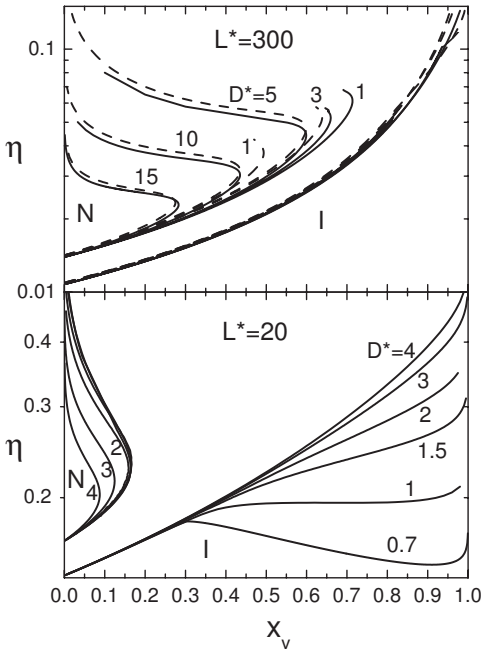

FIG. 4. Parsons-Lee (solid curves) and Onsager (dashed curves, top panel only) isotropic-nematic coexistence diagrams for HSC-HS fluids with fixed rod length of the HSC particles (L^*) and different diameter of the HS particles (D^*): Top panel: $L^*=300$ and $D^*=1-15$, bottom panel: $L^*=20$ and $D^*=0.7-4$.

ence diagram on the relative sizes of the HSC and HS particles. Figure 3 compares the *I-N* coexistence branches for HSC-HS fluids with different HSC elongations ranging $L^*=5-300$. As can be seen, the main features of the coexistence diagrams are similar for the different L^* values and reproduce the qualitative behavior observed in Fig. 1. In all cases, the isotropic states at low volume fractions of spheres coexist with nematic states with relatively small differences in x_v and η, although the nematic state is always appreciably poorer in spheres and displays systematically greater packing fractions. As the value of x_v grows in the isotropic branch, the differences in both x_v and η with the nematic branch vary progressively. Eventually, the system enters the demixing regime described above, in which nematic states rich in spherocylinders coexist with isotropic states rich in spheres. It is interesting to observe that the maximum value of x_v attained in the nematic branch before demixing occurs, shifts toward greater values of x_v as L^* grows for fixed D^*. This implies that the homogeneity of the isotropic and nematic phases, and hence the "resistance" of the system against demixing, in the HSC-HS fluid is enhanced with growing L^*. Such trend is a natural consequence of the dominance of the HSC-HSC pair interactions [e.g., the $v_{cc}(\gamma)$ term of Eq. (5)] in the high L^* limit, which tends to overrun the depletion effects that drive the demixing behavior. The greater weight of the pair HSC interactions is also responsible for the shift of the *I-N* coexisting branches globally toward smaller packing fractions with growing L^*.

Figure 3 shows that the coexistence diagram resulting from Onsager theory agrees well with the Parsons-Lee one only for the two cases of greater elongation $L^*=100$ and 300. On the contrary, the quantitative accuracy of the Onsager approximation deteriorates for smaller elongations and in particular for the three depicted fluids with $L^*=50$, 20, and 5. The bottom panel of Fig. 3 compares the coexistence pressure branches from Parsons-Lee and Onsager theory for two illustrative cases. Note that in this diagram the recognition of the coexisting states, both having the same pressure, is straightforward. The agreement between both theoretical approaches is better in the pressure diagram than in the packing fraction diagram, in particular for the $L^*=20$, $D^*=2$ case. Hence, Onsager estimation of coexisting pressures appears to be more robust than that of packing fractions. Overall, we found that Onsager results for the isotropic-nematic coexistence of the HSC-HS fluid diverged appreciably from their Parsons-Lee counterparts in general for fluids with $L^*<100$. For elongations of the HSC particles greater than $L^*=100$, Onsager theory provided reliable results except in regions of the phase diagram involving volume fractions of spheres too close to unity, as further shown below.

Figure 4 depicts the dependence of the *I-N* coexistence diagram with the diameter of the spherical particles for two fixed HSC elongations, namely, $L^*=300$ and 20. For the fluids with $L^*=300$ the coexistence curves from both Onsager and Parsons-Lee theories are shown for comparison. For the $L^*=20$ fluids only the Parsons-Lee (PL) theory is considered. Irrespectively of whether the Onsager or the PL approach was employed, the computations for $L^*=300$, $D^*\leqslant 3$ could be calculated up to neatly beyond the reversal of the nematic branch toward the demixed regime. However, a point beyond

which no converged results could be obtained was eventually reached. It will be discussed below that the observed lack of convergence in the demixing region of the *I-N* curves may be attributed to the entrance of the system into a *N-N* coexistence region.

One of the main conclusions that can be drawn from the results of Fig. 4 is that the stability of the mixed *I-N* coexistence is reduced with the increase in size of the spherical component in the binary mixture. According to the PL calculation, for $L^*=300$ and increasing $D^*=1$, 3, 5, and 15, *I-N* states coexist under mixed conditions up to progressively smaller HS volume fractions, of $x_v=0.71$, 0.66, 0.60, and 0.28, respectively. For $L^*=20$, a similar trend is found, although in this case the transitions to the demixing regime takes place at roughly the same $x_v \approx 0.165$ within $D^*=0.7-1.5$, with a shallow maximum of $x_v \approx 0.167$ for $D^*=1.25$. This same behavior was found for $L^*=5$ (not shown) where the turning point into the demixing regime is delayed to $x_v \approx 0.83$ for $D^*=1.5$, in comparison to $x_v \approx 0.72$ for both $D^*=1$ and 2. Such weak dependence of the demixing transition on the size of the spherical articles in the region of small D^* values, even featuring a non-monotonous character, appears to be reminiscent of the excluded volume contributions contained in the second order virial terms of the free energy. In fact, Onsager theory predicts a much more pronounced nonmonotonous dependence on D^* of the stability of the mixed regime. Within the Onsager approximation, for the $L^*=300$ fluid the demixing regime enters, for instance, at $x_v=0.49$, 0.64, 0.60, and 0.27 for $D^*=1$, 2, 3, and 15, with a detailed computation showing that the range of stability of the mixed *I-N* coexistence becomes indeed maximum for $D^* \approx 3$. This is the reason for the strong discrepancy between the Onsager and Parsons-Lee coexistence curves for the $L^*=300$, $D^*=1$ fluid that can be appreciated in Fig. 4.

A further remarkable aspect illustrated in Fig. 4 is the appreciable maximum in η displayed by the isotropic branch of the $L^*=20$ fluid in the small D^* limit. Such trend is observed for $D^* \leqslant 1$ and indicates that the expel of HSC particles from the isotropic phase as the system enters the demixing regime leads to a less efficient packing of the fluid in that phase. A similar behavior of the isotropic branch for small D^* was observed for $L^*<20$, as illustrated in Fig. 1 for $L^*=5$. As the volume of the HS particles becomes comparable or greater than that of the HSC particles, this effect vanishes and the packing fraction isotropic branch increases monotonously over the whole x_v range. In fact, for the mixtures with $L^*=20$ and $D^*>2$, the packing fraction of the isotropic branch for x_v close to unity reaches values typical of the solid phase of the bulk HS system. Hence, these latter cases correspond to a situation in which the HS particles freeze upon segregation from the HSC particles. The pertinence of this remark is related to the experimental observation of a similar type of behavior reported by Fraden and co-workers for mixtures of rodlike viruses and spherical colloids [33]. In these experiments the colloids were found to form arrangements of solidlike filaments segregated from the bulk of nematic viruses. This phenomenology, still without a clear explanation, presents similarities with the nematic HSC-solid-HS phase separation described here.

Figure 5 illustrates the stability of the isotropic and nematic phases against *I-I* and *N-N* demixing transitions. This is

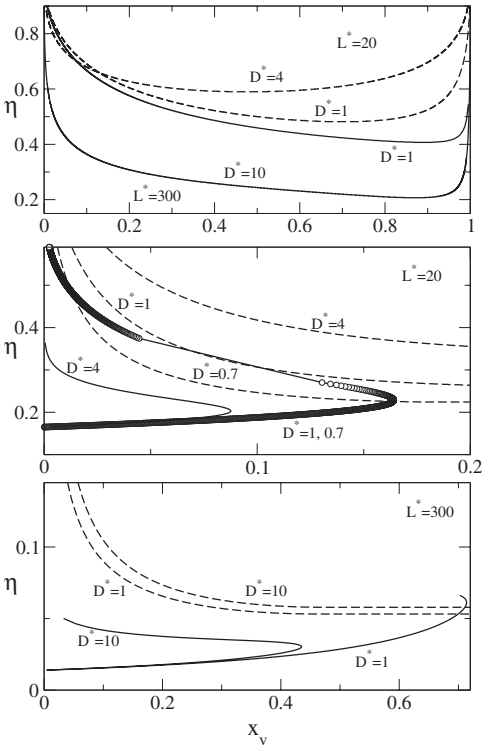

FIG. 5. Top panel: isotropic-isotropic spinodal demixing curves for HSC-HS fluids with $L^*=300$, $D^*=1$ and 10 (solid curves) and $L^*=20$, $D^*=1$ and 4 (dashed curves). Middle panel: Nematic-nematic spinodal demixing curves (dashed lines) for HSC-HS fluids with $L^*=20$, $D^*=0.7$, 1, and 4. The corresponding nematic branches of the *I-N* coexistence are also included for direct comparison. Note the discontinuity in the *I-N* curve for $D^*=0.7$ (symbols) not present in the closely overlapping curve for $D^*=1$ (solid line). Bottom panel: Same as middle panel but for $L^*=300$, $D^*=1$ and 10. The *I-I* or *N-N* demixing transitions can take place at packing fractions above the corresponding spinodals.

done by means of the Parsons-Lee spinodal curves resulting from the mapping on the x_v-η plane of the conditions defined in Eq. (16). Demixing could take place if the packing fractions associated to the corresponding spinodal become smaller than the packing fractions obtained for *I-N* coexistence. Spinodals for *I-I* demixing were computed for HSC aspect ratios ranging $L^*=5-1000$ and HS diameters up to $D^*=1000$. Figure 5 shows only some illustrative examples. The detailed analysis of these spinodals indicates that *I-I* coexistence becomes feasible for sufficiently large D^* values, namely, e.g., $D^*>4$, 6, 10, 20, 30, and 90 for $L^*=5$, 10, 20, 100, 300, and 1000, respectively. It can be noted that these HS diameters are significantly greater than the ones considered above for the *I-N* coexistence and therefore do not interfere with the diagrams of Figs. 2–4. This conclusion is supported by the fact that our algorithm never converged to a *I-N* coexistence configuration of low orientational order in the *a priori* nematic phase. This type of convergence would have been plausible, since the $h(\theta)$ distribution was free to adjust through its Legendre coefficients to the configuration of minimum free energy. This result is also consistent with the prediction outlined in Ref. [54] that for sufficiently long

rods, *I-I* demixing becomes only stable for comparably large sphere sizes.

The *N-N* Parsons-Lee spinodals for different HSC-HS molecular sizes are shown in the lower panels of Fig. 5. The corresponding nematic branches of the *I-N* coexistence curves are also shown for comparison. In this case, the computation of the spinodals from the conditions of Eq. (16) involves the iterative optimization of $h(\theta)$ for each HS volume fraction and packing fraction of the mixture through Eqs. (13) and (14). For the mixtures involving HSC particles with $L^*=20$ (middle panel of Fig. 5), the comparison with the *I-N* coexistence curves indicates that for $D^* \geqslant 1$, *N-N* demixing requires too large packing fractions and is therefore unstable with respect to *I-N* demixing within the Parsons-Lee approximation. Only for $D^*<1$ would the *N-N* phase separation be allowed, so that the present results for *I-N* equilibrium for this range of geometries should be considered with caution. Interesting, the nematic branch of the *I-N* coexistence curve for $L^*=20$, $D^*=0.7$ displays a discontinuity after the turning point (i.e., already within the domain of demixing) where a small change in the composition of the isotropic branch induces an abrupt change in both the composition and packing fraction of the coexisting nematic state. It is interesting to notice that the appearance of such discontinuity is coincident with the evolution of the spinodal to packing fraction values neatly below those of the *I-N* curve. It would therefore be plausible that the range of the composition-packing fraction diagram not covered by the *I-N* curve corresponds to the domain of stability of *N-N* coexistence. This expectation is consistent with the description of the overall phase diagram given by Lekkerkerker and Stroobants [54].

For the case of HSC particles with $L^*=300$ (bottom panel of Fig. 5), *I-N* coexistence is favored in all cases with $D^* \geqslant 5$. This is illustrated by the comparison for $D^*=10$ showing that too large η values are required for *N-N* equilibrium. For smaller sizes of the HS particles, represented by $D^*=1$ in Fig. 5, a composition domain appears in which *N-N* separation competes favorably, according to the smaller η of the spinodal with respect to the nematic branch of the *I-N* coexistence. Such a situation arises only for sufficiently high values of x_v (i.e., for large molar fractions of the HS particles), whereas for low values of x_v the *I-N* separation remains stable. In this case, the entrance of the possible *N-N* demixing takes place in a region where the algorithm to calculate the *I-N* coexistence did not converge to any solution (see Fig. 4). Such lack of convergence is likely to be related to a discontinuous gap in the nematic branch similar to the one described above for the case $L^*=20$, $D^*=0.7$. In this case, however, the boundary nematic states are too different from each other to be linked by the genetic algorithm employed in the present work. This interpretation then suggests the entrance of the fluids $L^*=300$, $D^* \leqslant 3$ in the *N-N* coexistence region at some point after the turning point of the *I-N* branch.

A modification of the present methodology considering independent $h(\theta)$ distributions for the coexisting phases (i.e., allowing *N-N* equilibrium) led to the same *I-N* coexisting curves within the range of convergence of the original algorithm (one of the orientational distributions became isotropic). However, the algorithm did not reach convergence for the pressures and chemical potentials within the expected domain of *N-N* stability. In conclusion, in order to characterize in a more complete way the phase diagram of HSC-HS mixtures, an extended investigation would be required. Such investigation, in addition to implementing an efficient algorithm to characterize in detail the *N-N* coexistence binodals should incorporate the lamellar phase into the treatment. This lies beyond the aim of the present work, where the domain of stability of the *I-N* coexistence diagram has been determined for particle sizes where the lamellar phase is not expected to interfere. For these cases, the region where *N-N* separation may become stable within the Parsons-Lee approximation have been established (e.g., $L^*=20$, $D^*<1$ or $L^*=300$, $D^* \leqslant 3$ for sufficiently high x_v values).

Figure 6 represents the Parsons-Lee equations of state at constant mixture composition (isopleths) for rod-sphere mixtures with $L^*=20$ and $D^*=1,2,4$ and with $L^*=300$ and $D^*=2,5,7$. The range of volume fractions of spheres considered in each case corresponds to the region of relatively small composition asymmetry in the coexisting *I-N* diagram (see Fig. 3). Such region lies before the entrance of the system into the demixed regime and sufficiently anticipated with respect to the region where *N-N* separation may become relevant. The different isopleths show the expected positive correlation between pressure and packing fraction. The displacement of the *I-N* transition toward greater η values with growing x_v (i.e., destabilization of the nematic phase by the depletion effects induced by the spherical component) can also be appreciated, as already noticed above in the coexistence diagrams. For the smaller HS diameters considered in Fig. 6 it is observed that the system pressure increases appreciably with growing x_v in both the *I* and *N* phases (at fixed η). This behavior, also found in Monte Carlo simulation studies [43], occurs as a natural consequence of the multiplication of the number density of the system with any increase of x_v. This in turn follows from the much smaller volume of the spherical particles in comparison to the rods. The opposite effect is observed for sufficiently large HS diameters once the HS molecular volume becomes greater than the HSC one. In this case, any increase in the volume fraction of spheres, for fixed η, leads to a decrement in the absolute number of particles per unit volume and, hence, to a decrease in the system pressure.

Interestingly, for intermediate D^* values, where the HS and HSC molecular volumes become comparable, a situation arises where the composition has a weak effect on the pressure-packing fraction representation of the isopleth. This is a consequence of the effective compensation of the excluded volume contributions that drive the system pressure. Moreover, Fig. 6 shows that such steric effects vary significantly from the isotropic to the nematic phase so that it is possible to find roughly composition-independent isopleths in one phase and appreciable composition effects on the other phase. In fact, for the mixtures $L^*=20$, $D^*=2$ and $L^*=300$, $D^*=5$, whereas a close overlap is found for the isopleths with the different x_v values in the isotropic phase, a significant shift of pressure with x_v is still observed in the nematic phase. The complementary situation of an almost negligible dependence on x_v of the isopleths in the nematic

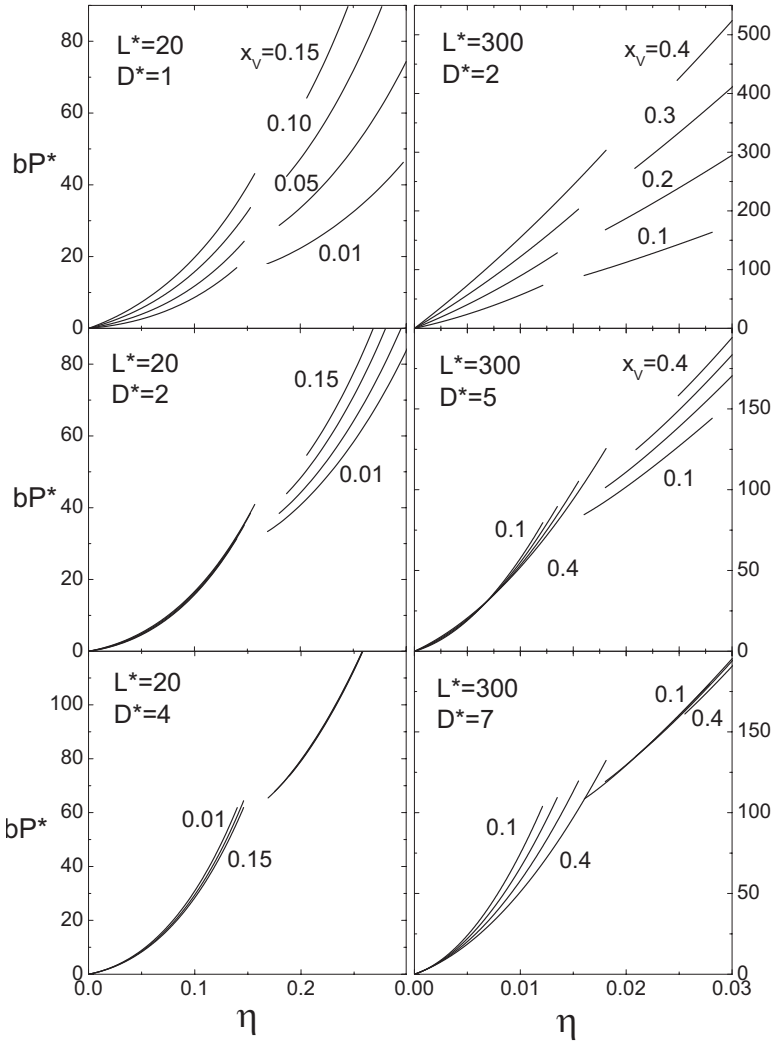

FIG. 6. Equations of state at constant composition (isopleths) predicted by Parsons-Lee theory for the isotropic and nematic phases of binary HSC-HS mixtures with fixed $L^*=20$ and 300 and different HS diameters D^*. The indicated values for the volume fraction of spheres x_v correspond to the mixed regime of the two phases (see Fig. 3 for reference). The dimensionless pressure bP^* is defined as in Fig. 3.

phase is found for $L^*=20$, $D^*=4$ and $L^*=300$, $D^*=7$. It is worthwhile noticing that the weakest composition dependence of the isopleths in the isotropic phase is found, in both the $L^*=20$ and $L^*=300$ mixtures, for molecular volume ratios between the HS and HSC particles of $v_s/v_c \approx 0.25$. On the other hand, for the nematic phase, this situation is found for $v_s/v_c \approx 2$ for $L^*=20$ and $v_s/v_c \approx 0.75$ for $L^*=300$. These values are in contrast to the common choice of $v_s=v_c$ (i.e., $D^*=3.1$ for $L^*=20$ and $D^*=7.7$ for $L^*=300$), often employed when the HS fluid is taken as reference system for the HSC fluid in approximate theories. In any case, only for mixtures involving relatively short rods it seems possible to find an effective value of D^* for which the isopleth of the mixture becomes insensitive to the composition of the mixture simultaneously in the isotropic and the nematic phases.

Simulation or experimental studies of the equation of state (EOS) of HSC-HS mixtures, that could provide a reference for the evaluation of the present theoretical results, are scarce. Isopleths for the isotropic and nematic phases have been reported in previous works from *NPT*-MC simulations for the $L^*=5$, $D^*=1$ fluid [43]. For the present paper, we have extended those simulations to include the case $L^*=5$, $D^*=3$ employing the same methodology described in Ref. [43]. Figure 7 illustrates the level of agreement observed between the Parsons-Lee isopleths in the isotropic and nematic phases and the results from *NPT*-MC simulations for these particular cases. In addition, alternative EOS for the isotropic phase of the HSC-HS system from scaled particle theory proposed by other authors [56,57] are also shown. It can be appreciated that these latter EOSs, originally developed for shorter HSC molecules, remain fairly accurate at the $L^*=5$ elongation considered. Nevertheless, the EOS from Parsons-Lee theory compares better with the simulation data than any of the curves from scaled particle theory. Similar or better level of accuracy for the Parsons-Lee EOS can be expected for mixtures with greater L^* values. In the immediacy of the isotropic-nematic transition and in the nematic phase itself, although Parsons-Lee theory compares fairly well with simulation, the agreement is worse than in the isotropic phase. This can be attributed to the intrinsic limitations of the Parsons-Lee approximation to manage orientational order. In fact, the Parsons-Lee results presently obtained for the nematic phase of HSC-HS mixtures, show a similar accuracy when compared to MC data as found for the pure HSC fluid [48].

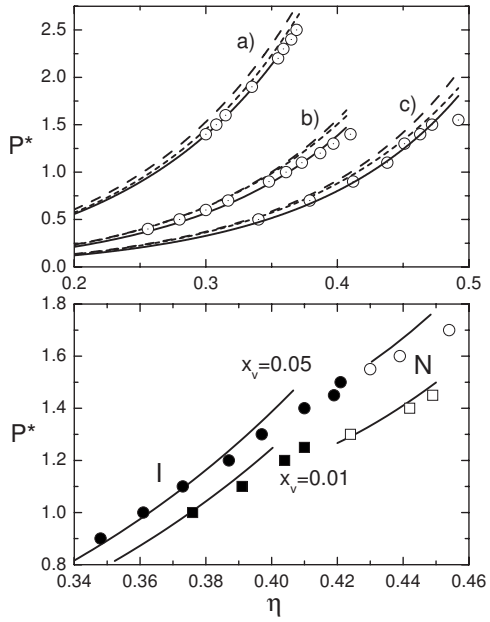

FIG. 7. Comparison between theory and simulation for EOS of HSC-HS fluids. Top panel: Isotropic phase EOS for (a) $L^*=5$, $D^*=1$ with $x_v=0.536$, (b) $L^*=5$, $D^*=1$ with $x_v=0.05$, (c) $L^*=5$, $D^*=3$ with $x_v=0.320$. Solid curves correspond to the Parsons-Lee EOS, whereas dashed curves and dotted curves are predictions from scaled particle theory (from Refs. [56,57], respectively). Circles are the *NPT*-Monte Carlo data. All curves converge to zero density in the zero pressure limit (not shown). Bottom panel: EOSs obtained by PL theory (solid curves) and Monte Carlo simulation in the isotropic (full symbols) and nematic (open symbols) phases for HSC-HS fluid with $L^*=5$ and $D^*=1$ for $x_v=0.01$ and 0.05. Note that $P^*=\beta P\sigma^3$.

IV. FINAL REMARKS AND CONCLUSIONS

The extension of the Parsons-Lee and Onsager theories for the isotropic-nematic transition in binary mixtures of hard spherocylinders and hard spheres has been outlined in a compact way. Both theories become exact in the limit of very long rodlike particles. Onsager theory remains accurate for rod length values of $L^*\approx 100$ or greater, with some general limitations for mixtures with large molar fractions of the spherical particles. Parsons-Lee theory yields qualitatively correct results for rods as short as $L^*\approx 5$-20.

The following trends are predicted which are in general qualitative agreement with experimental observations and with the result of more complex theories.

(1) The isotropic-nematic transition of a system of rodlike molecules is delayed toward greater packing fractions with the addition of spherical depletion agents, thereby perturbing the rod-rod interaction which drives the *I*-*N* transition. It can be noticed that this effect is opposite to that found previously for the nematic-smectic transition, which takes place at packing fractions significantly greater than the ones presently considered, and lies outside the scope of the current work [43–45].

(2) For a sufficiently large volumetric fraction of spheres x_v in the system, the partitioning between the isotropic and nematic phases eventually becomes highly asymmetric. The coexistence diagram of the binary mixture evolves from a region at low x_v with relative small differences in composition between the *I* and *N* states, to a demixing regime, where x_v becomes much larger in the isotropic phase than in the nematic phase. The appearance of highly partitioned isotropic-nematic coexistence diagrams in qualitative agreement with the present Onsager and Parsons-Lee theories has been observed experimentally [19,32,33,35–41] and has been described by theoretical treatments at different levels of accuracy [19,54].

(3) The quantitative features of the *I*-*N* coexistence diagram and, in particular, the entrance into the demixing region can be controlled with the appropriate size of the rodlike and the spherical particles. On one hand, increasing the length of the HSC particles favors the stability of the well mixed nematic phase. A similar overall effect is found when decreasing the size of the HS particles. However, the influence of D^* on the entrance of the system into the demixed regime presents some subtle behavior: Parsons-Lee theory predicts a weak dependence of the demixing transition on the size of the spherical articles in the region of small D^* values, with even a slight nonmonotonous character, for the mixtures with $L^*\leqslant 20$. Such behavior appears to be reminiscent of the second order virial free energy terms associated to excluded volume contributions. In fact, Onsager theory predicts a much more pronounced (and overestimated) nonmonotonous dependence on D^* of the stability of the mixed regime. To our knowledge, this aspect has not been explicitly addressed experimentally, but it should be of practical interest in colloidal science.

(4) The computation of the Parsons-Lee spinodals indicates that *I*-*I* separation becomes stable for HS diameters much greater than those involved in the *I*-*N* coexistences relevant to the present work (e.g., $L^*=20$, $D^*>10$ or $L^*=300$, $D^*>30$). On the other hand, *N*-*N* demixing may indeed become stable for sufficiently long rods and small spheres (e.g., $L^*=20$, $D^*<1$ or $L^*=300$, $D^*\leqslant 3$). For these particle geometries, *N*-*N* demixing may occur in a region of the phase diagram beyond or close to the demixing region of the *I*-*N* coexistence.

(5) The relative size of the HS and HSC particles also determines the dependence of the isoplethic equation of state on the composition of the mixture. For intermediate L/D ratios a situation is encountered where the excluded volume contributions associated to the HSC-HSC, HS-HS, and HSC-HS pair interactions compensate each other, with the consequence that the composition has a weak effect on the pressure *versus* packing fraction representation of the isopleth. This is in contrast to the case of large sphere-rod size asymmetry, where significant changes in pressure are observed in the system when varying its composition at a given constant packing fraction. The dependence of the EOS on the mixture composition may vary considerably from the isotropic to the nematic phase. It is possible to have a virtual overlap of the isopleths in one phase and appreciable differences in the other phase. In other words, the choice of a binary mixture with a specific effective size ratio cannot be expected to eliminate the composition dependence of the EOS in both phases simultaneously.

(6) Parsons-Lee theory yields more accurate EOSs for the isotropic phases of the HSC-HS system than any other ap-

proach reported in the literature. It also provides the EOS in the nematic phase in fair agreement with simulation results for the systems tested in the present work.

We have shown that a simple extension of the Parsons-Lee and Onsager theories serves well to rationalize and predict the general phase behavior of binary mixtures of spherical colloids and rodlike nematogens.

ACKNOWLEDGMENTS

Financial support is acknowledged from the Ministry of Education and Science of Spain (Projects No. CTQ2004-07730-C02 and No. VEM2003-20574-C03) and from the Regional Government of Andalusia (groups PAI FQM-205 and FQM-319). A.C. acknowledges support from the Nederlandse Organisiate voor Wetenschappelijk Onderzoek.

APPENDIX: GENETIC ALGORITHM

Solving the isotropic-nematic coexistence problem within Parsons-Lee or Onsager theory implies the solution of a nonlinear system of equations associated to the mechanical and chemical equilibria of the two phases. Such a general problem can be expressed by means of the vector equation

$$\mathbf{H}(\mathbf{x}) = 0, \tag{A1}$$

where the vectors $\mathbf{H}$ and $\mathbf{x}$ represent a set of n nonlinear equations and the n uncertainties, respectively. Iterative methods treat the above equation in an approximate way:

$$|\mathbf{H}(\mathbf{x})| < \delta, \tag{A2}$$

where δ is the tolerance of the solution method.

The philosophy behind the so-called genetic algorithms [59,60] relies on the concepts outlined by Darwin for the evolution of the species, brought to the level of genome evolution. The method considers a population of n_g possible vector solutions to Eq. (A2), each of which is called a chromosome. Chromosomes are then vectors, whose components are particular values of the uncertainties of the problem (in the present case, η_I, η_N, and x_c^N); each of such components is called a gene.

A population of $n_g=3000$ chromosomes is considered and ranked according to the value of $|\mathbf{H}(\mathbf{x})|$. The population is allowed to evolve in a way that ensures that those chromosomes closer to the solution of the problem have greater survival and reproduction probabilities. In the initial step, the population $\{\mathbf{x}(n;n_g)\}$ is generated randomly. Subsequent generations are obtained according to the following sequence.

The 65% best chromosomes of the population are kept unchanged in the new generation.

10% of the chromosomes of the new population are generated by averaging the genes of two chromosomes among the best 20% of the previous generation.

Another 10% of the new population is generated by modifying by less than 0.5% the value of some of the genes of chromosomes among the best 50% of the previous generation.

One further 10% of new chromosomes is generated by interchanging some of the genes of two chromosomes among the best 50% best of the previous generation.

Finally, the remaining 5% of the new chromosomes are generated by changing by more than 5% the value of one gene of one of the original chromosomes.

In all the above cases, the chromosomes and genes to be altered are chosen at random

For the present application, where the genes represent packing fractions and molar fractions, the physical restriction $0<x(i)<1$ is imposed on the evolution rules described above. The evolution procedure is carried out iteratively yielding new generations through 1000 iterations. The iteration is interrupted if the best chromosome of the population fulfilled $|\mathbf{H}|<\delta$, with $\delta=10^{-5}$. The set of genes of this chromosome is then taken as solution of the system of equations.

In the present method (see Sec. II), the solution to the coexistence equilibrium problem $[\mathbf{H}(\mathbf{x})=0]$ is coupled with the determination of the orientation distribution function $h(\theta)$ [Eq. (14)]. The solution to the overall problem is accepted when a best chromosome is achieved for which $|\mathbf{H}|<\delta$ and simultaneous self-consistent convergence has been obtained in the a_n expansion coefficients of $h(\theta)$. The different parameters of the algorithm (distribution of the changes, tolerances, etc.) have been chosen after several trials as to provide the optimum compromise between accuracy and convergence speed. In comparison with the well known (and faster) Newton-Raphson method, the present genetic algorithm provided coincident results in the region of the phase diagram where both methods converged, but extended significantly the domain of convergence, especially for mixtures involving short HSC particles ($L^*<100$).

[1] J. Herzfeld, Acc. Chem. Res. **29**, 31 (1996).
[2] R. J. Ellis and A. Minton, Nature (London) **425**, 27 (2003).
[3] L. Onsager, Ann. N.Y. Acad. Sci. **51**, 627 (1949).
[4] W. Maier and A. Saupe, Z. Naturforsch. A **13**, 564 (1958); **15**, 287 (1960).
[5] H. N. W. Lekkerkerker, Ph. Coulon, and R. Van Der Haegen, J. Chem. Phys. **80**, 3427 (1984).
[6] R. F. Kayser and H. J. Raveché, Phys. Rev. A **17**, 2067 (1978).
[7] T. Odijk, Liq. Cryst. **1**, 97 (1986).
[8] T. Odijk, Macromolecules **19**, 2313 (1986).
[9] D. Frenkel, J. Phys. Chem. **91**, 4912 (1987); **92**, 5314(E) (1988).
[10] G. J. Vroege and H. N. W. Lekkerkerker, Rep. Prog. Phys. **55**, 1241 (1992).
[11] T. M. Birshtein, B. I. Kolegov, and V. A. Pryamitsyn, Polym. Sci. U.S.S.R. **30**, 316 (1988).
[12] R. van Roij and B. Mulder, Phys. Rev. E **54**, 6430 (1996).
[13] H. H. Wensink and G. J. Vroege, J. Chem. Phys. **119**, 6868

(2002).
[14] S. Varga, K. Purdy, A. Galindo, S. Fraden, and G. Jackson, Phys. Rev. E **72**, 051704 (2005).
[15] F. M. van der Kooij and H. N. W. Lekkerkerker, J. Phys. Chem. B **102**, 7829 (1998).
[16] F. M. van der Kooij and H. N. W. Lekkerkerker, Phys. Rev. Lett. **84**, 781 (2000).
[17] J. P. Hansen and I. R. McDonald, *Theory of Simple Liquids*, 3rd ed. (Academic Press, London, 2006).
[18] P. Tarazona, Philos. Trans. R. Soc. London, Ser. A **345**, 307 (1993).
[19] Z. Dogic and S. Fraden, in *Soft Matter*, edited by G. Gompper and M. Schick (Wiley-VCH, Weinheim, 2005), Vol. 2.
[20] J. D. Parsons, Phys. Rev. A **19**, 1225 (1979).
[21] S. D. Lee, J. Chem. Phys. **87**, 4972 (1987).
[22] M. A. Cotter and D. C. Wacker, Phys. Rev. A **18**, 2669 (1978).
[23] G. Cinacchi, E. Velasco, and L. Mederos, J. Phys.: Condens. Matter **16**, S2003 (2004).
[24] G. Cinacchi, L. Mederos, and E. Velasco, J. Chem. Phys. **121**, 3854 (2004).
[25] Y. Martínez-Ratón, E. Velasco, and L. Mederos, J. Chem. Phys. **123**, 104906 (2005).
[26] S. Varga, A. Galindo, and G. Jackson, J. Chem. Phys. **117**, 7207 (2002); **117**, 10412 (2002).
[27] G. A. Vliegenthart and H. N. W. Lekkerkerker, J. Chem. Phys. **111**, 4153 (1999).
[28] G. H. Koenderink, G. A. Vliegenthart, S. G. J. M. Kluijtmans, A. P. Philipse, and H. N. W. Lekkerkerker, Langmuir **15**, 4693 (1999).
[29] J. M. Brader, A. Esztermann, and M. Schmidt, Phys. Rev. E **66**, 031401 (2002.).
[30] N. Urakami and M. Imai, J. Chem. Phys. **119**, 2463 (2003).
[31] P. Bolhuis, J. Brader, and M. Schmidt, J. Phys.: Condens. Matter **15**, S3421 (2003).
[32] S. Fraden, in *Observation, Prediction and Simulation of Phase Transitions in Complex Fluids*, edited by M. Baus, L. F. Rull, and J. P. Ryckaert (Kluwer Academic Publishers, Dordrecht, 1995).
[33] M. Adams, Z. Dogic, S. L. Keller, and S. Fraden, Nature (London) **393**, 349 (1998).
[34] M. Adams and S. Fraden, Biophys. J. **74**, 669 (1998).
[35] Z. Dogic and S. Fraden, Philos. Trans. R. Soc. London, Ser. A **359**, 997 (2001).
[36] Z. Dogic, K. R. Purdy, E. Grelet, M. Adams, and S. Fraden, Phys. Rev. E **69**, 051702 (2004).
[37] C. D. Edgar and D. G. Gray, Macromolecules **35**, 7400 (2002).
[38] J. Buitenhuis, L. N. Donselaar, P. A. Buining, A. Stroobants, and H. N. W. Lekkerkerker, J. Colloid Interface Sci. **175**, 46 (1995).
[39] J. C. Loudet and Ph. Barois, Nature (London) **497**, 611 (2000).
[40] K. Inomata, N. Ohara, H. Shimizu, and T. Nose, Polymer **39**, 3379 (1998).
[41] E. Bianchi, A. Ciferri, and A. Tealdi, Macromolecules **15**, 1268 (1982).
[42] M. Ramzi, J. Borgström, and L. Piculell, Macromolecules **32**, 2250 (1999).
[43] S. Lago, A. Cuetos, B. Martínez-Haya, and L. F. Rull, J. Mol. Recognit. **17**, 417 (2004).
[44] T. Koda, M. Numajiri, and S. Ikeda, J. Phys. Soc. Jpn. **65**, 3551 (1996).
[45] Z. Dogic, D. Frenkel, and S. Fraden, Phys. Rev. E **62**, 3925 (2000).
[46] D. Antypov and D. J. Cleaver, J. Chem. Phys. **120**, 10307 (2004).
[47] S. Varga, A. Galindo, and G. Jackson, Mol. Phys. **101**, 817 (2003).
[48] S. C. McGrother, D. C. Williamson, and G. Jackson, J. Chem. Phys. **104**, 6755 (1996).
[49] D. C. Williamson and G. Jackson, Mol. Phys. **83**, 603 (1994).
[50] M. Franco-Melgar, Ph.D. thesis, Imperial College, London, 2005.
[51] A. Cuetos, B. Martinez-Haya, S. Lago, and L. F. Rull, J. Phys. Chem. B **109**, 13729 (2005).
[52] K. Lakatos, J. Stat. Phys. **2**, 121 (1970).
[53] P. J. Flory, Macromolecules **11**, 1138 (1978).
[54] H. N. W. Lekkerkerker and A. Stroobants, Nuovo Cimento D **16**, 949 (1994).
[55] H. H. Wensink and G. J. Vroege, J. Phys.: Condens. Matter 16, (2004).
[56] T. Boublik, Mol. Phys. **42**, 209 (1981).
[57] C. Barrio and J. R. Solana, J. Chem. Phys. **111**, 4640 (1999).
[58] P. Bolhuis and D. Frenkel, J. Chem. Phys. **106**, 666 (1997).
[59] J. H. Holland, *Adaption in Natural and Artificial Systems* (University of Michigan Press, Ann Arbor, 1975).
[60] D. A. Coley, *An Introduction to Genetic Algorithms for Scientists and Engineers* (World Scientific, Singapore, 1999).